Harmonic performance of heat-pumps

W.J.B. Heffernan[1], N.R. Watson[2], R. Buehler[3], J.D. Watson[2]

[1]*Electric Power Engineering Centre, University of Canterbury, Christchurch 8140, New Zealand*
[2]*Electrical and Computer Engineering Department, University of Canterbury, Private Bag 4800, Christchurch 8140, New Zealand*
[3]*ABB Ltd., Brown-Boveri-Strasse 5, CH-8050, Zurich, Switzerland*
E-mail: Neville.Watson@canterbury.ac.nz

Published in *The Journal of Engineering*; Received on 16th April 2013

Abstract: Reverse cycle air-source heat-pumps are an increasingly significant load in New Zealand and in many other countries. This has raised concern over the possible impact wide-spread use of heat-pumps will have on the grid. To analyse this impact, models are needed to enable system studies to be performed. In this paper, the results from testing six heat-pumps are presented. The heat-pumps are classified based on observed performance. Moreover, the heat-pumps' designs are investigated and power system computer aided design/electromagnetic transient program for DC (PSCAD/EMTDC) models developed and verified against the measured performance.

1 Introduction

Heat-pumps (referred to as air conditioners in the standards) are being deployed throughout New Zealand at a very fast rate. This is driven largely by the demand for more efficient electric heating, as well as the desire to replace solid fuel burners for environmental reasons [1]. Moreover, the recent earthquakes in Canterbury have demolished most of the chimneys in the region and heat-pumps have been hastily installed to give much needed heating. In recent years, other countries have also experienced a large uptake of heat-pumps [2]. Early heat-pumps typically use directly connected induction motors, where a contactor turns the compressor motor on or off. These draw a large starting current, which can cause voltage dips. Modern heat-pumps, however, use inverter-driven induction motors to improve performance and only a few currently manufactured, low-end units still use directly connected induction motors. While the inverter drives increase efficiency and reduce inrush current, the rectifier circuits are a known source of harmonics. In order to meet international standards, some form of power factor correction (PFC) circuitry must be added to the basic rectifier circuit [3, 4]. The behaviour of the heat-pump as seen from the AC system depends largely on the particular PFC rectifier circuit used. Inverter-driven heat-pumps can exhibit a higher PF compared with directly connected induction motor heat-pumps [5–7].

This paper presents the results of tests to determine the PF and harmonic characteristics of six commercially available heat-pumps. Moreover, the various rectifier circuits of the five inverter-driven heat-pumps tested are studied and modelled. This is done to explain the laboratory test results and to provide a tool for simulating the effect of multiple heat-pumps connected to a feeder.

2 Heat-pump fundamentals

2.1 Heat-pump thermodynamics

Fig. 1 shows a simplified system diagram of a typical heat-pump. On the heating cycle the compression process heats the refrigerant, which then releases its heat to the surrounding air (the room) as it condenses in the indoor heat exchanger/condenser. The cooled liquid refrigerant then passes through an expansion valve into the outdoor heat exchanger/evaporator, where it evaporates back to the gaseous state, taking in heat from the surroundings in the process. On the cooling cycle the flow is reversed, the indoor heat exchanger is used as the evaporator and the outdoor exchanger becomes the condenser.

2.2 Motor drives

Earlier heat-pumps used a directly-connected induction motor (with an on/off contactor) to drive the compressor. However, the majority of new products use a power electronic inverter to supply the induction motor. Six heat-pumps were tested; the induction motor in five of these was inverter-driven, whereas in the sixth it was directly connected.

A PFC rectifier feeds a DC reservoir capacitor, from which the inverter drives a three-phase compressor motor. Using an inverter drive gives the following advantages:

- Variable speed control, which increases heat-pump controllability and efficiency.
- Soft-starting, which reduces starting current and hence light flicker.
- The PFC rectifier can be made to draw unity displacement PF (DPF), although this is not fully implemented in all inverter-driven heat-pumps.

Depending on the PFC rectifier implementation, some inverter-driven heat-pumps can draw significant harmonic currents.

2.3 Auxiliary circuits

For both inverter-driven and directly-connected (non-inverter) heat-pumps, in addition to the compressor motor there is electronic circuitry associated with monitoring the temperature of the ambient and refrigerant conditions, as well as blower fans to circulate air around the two heat exchangers. Hence, some electrical power is drawn even when the compressor is not running.

3 Heat-pump performance

Six heat-pumps were chosen, from five different manufacturers, as a representative sample of the heat-pumps available on the market. Five were inverter-driven (referred to henceforth as *A*25, *A*50, *B*, *D* and *E*), the sixth low-cost unit having a directly-connected induction motor (referred to as *C*). Units *A*50, *B*, *C*, *D* and *E* all have a similar nominal heating/cooling capacity (around 5 kW), whereas unit *A*25 (from the same manufacturer as *A*50) has a nominal heating/cooling capacity of about 2.5 kW.

This is an open access article published by the IET under the Creative Commons Attribution-NonCommercial License (http://creativecommons.org/licenses/by-nc/3.0/)

3.1 Energy efficiency

All heat-pumps placed on the market in Australia and New Zealand are required to be tested for energy efficiency according to standard AS/NZS 3823 [8]. This standard determines the efficiency by measuring the heating and cooling power output for rated electrical power input. These efficiencies are recorded as their energy efficiency rating (EER) and coefficient of performance (COP), where EER is the cooling efficiency and COP is the heating efficiency. For the six heat-pumps tested, the published efficiency data are shown in Table 1.

3.2 Harmonic testing

3.2.1 Test equipment: Two different voltage sources were used for testing the heat-pumps. The five inverter-driven heat-pumps were tested using two paralleled CHROMA programmable AC voltage sources. A motor-generator (MG) set was used to test unit *C*, because of the inability of the programmable AC voltage sources to supply the necessary starting current. For all tests on unit *C*, using the MG set, a voltage total harmonic distortion (V_{THD}) of less than 0.7% of fundamental was achieved.

The programmable AC sources connected in parallel are capable of supplying up to 14 A root mean square (RMS) and provide a very stiff sinusoidal source with a V_{THD} of less than 0.2% of fundamental.

All tests reported in this paper are at the nominal NZ supply voltage of 230 V RMS, 50 Hz and under steady-state operation. Although work covering behaviour during system dips, swells and transients and during heat-pump start-up has been carried out it is not reported here.

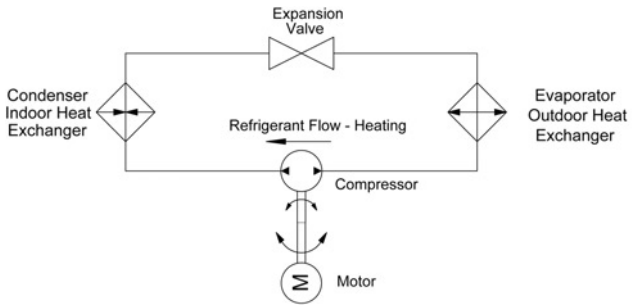


Fig. 1 *Simplified diagram of heat-pump in heating cycle*

Table 1 Heat-pump relative efficiency according to AS/NZS 3823

Model	Output power, kW		Input power, kW		COP/EER	
	Heat	Cool	Heat	Cool	COP	EER
*A*25	3.4	2.5	0.83	0.6	4.10	4.17
*A*50	5.8	5.0	1.6	1.55	3.63	3.23
B	6.25	5.2	1.73	1.72	3.61	3.02
C	5.6	4.8	1.90	1.70	2.95	2.82
D	5.6	5.0	1.70	1.66	3.29	3.01
E	5.5	4.4	1.57	1.37	3.50	3.21

It should be noted that these results are obtained with a special calibrated test facility and, most importantly, the input power is averaged over a considerable time period. At any given moment, the heat-pump may be drawing either more or less than the input power stated in Table 1 for the relevant cycle. The actual power drawn is dependent on various factors including the ambient conditions around the two heat exchangers and the temperature and phase of the refrigerant. This is the reason for the arbitrarily chosen set of real power levels shown in the results in this paper.

3.2.2 Harmonic limits: Harmonic currents are undesirable; therefore standards exist to limit the allowable harmonic emission of devices. The relevant standard is joint Australian and New Zealand standard AS/NZS 61000.3.2 (for devices with maximum RMS current of ≤16 A per phase) [4] which is essentially the same as the equivalent International Electrotechnical Commission (IEC) standard [3], but with the inclusion of an additional clause. The heat-pumps tested fall within the standard's category of Class *A* devices.

3.3 Harmonic results

Figs. 2–7 display the current waveforms for each of the six heat-pumps, on both heating and cooling cycles, at nominal voltage, for various power levels. For heating mode, it can be seen that:

- As expected, the directly-connected induction motor heat-pump (*C*) exhibits a relatively sinusoidal load current with a low harmonic content, although it does exhibit some second harmonic current.
- Some inverter-driven heat-pumps, classified later in this paper as Type 1 (*A*25, *B* and *E*) and Type 2 (*A*50), draw high harmonic currents, especially at low-power levels, with a distinct change in current waveshape above a certain power level.
- Unit *D* (Type 3) draws relatively low harmonics at all power levels.

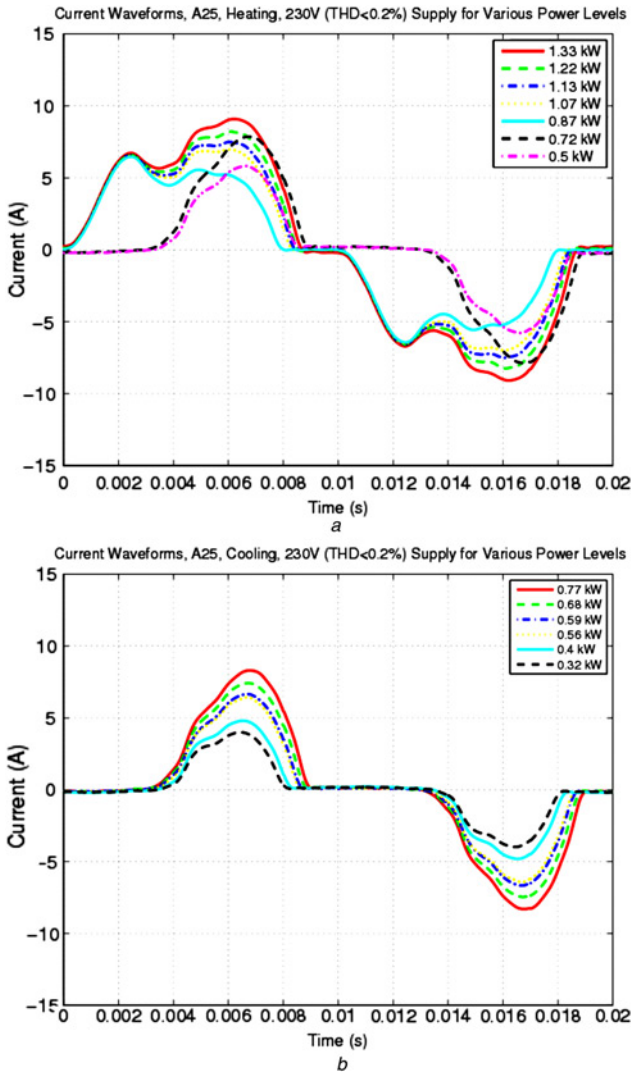


Fig. 2 *Heat-pump A25 current waveforms*
a Heating
b Cooling

This is an open access article published by the IET under the Creative Commons Attribution-NonCommercial License (http://creativecommons.org/licenses/by-nc/3.0/)

doi: 10.1049/joe.2013.0012

The spectra (showing the first 19 odd harmonics) of the current waveforms for unit *A*25, while heating, are shown in Fig. 8*a*, along with the relevant harmonic limits. These results give the strong impression that this particular unit was designed to just pass the third (at low power) and fifth (at high power) harmonic regulations. Nevertheless, the unit satisfies the standard up to and including the 40th harmonic.

The harmonic content when the heat-pumps are in the cooling cycle is similar to that exhibited in the heating cycle. Spectra for unit *A*50, while cooling, are displayed in Fig. 8*b*. Although the harmonic currents exceed the AS/NZS 61000.3.2 limits for odd-order harmonics between 5 and 19, when operating at low power levels, the heat-pump still complies with the standard, as compliance is only tested at rated power.

3.4 Crest factor

The current crest factor (CCF), which is the ratio of peak-to-RMS current, was recorded for all the operating conditions displayed in Figs. 2–7. It is significantly higher than $\sqrt{2}$ (1.41) for some units, when operating at low-to-medium powers. A CCF of 3.2 was reached for *A*50 at low power. There was an abrupt change in *A*50's characteristics at a certain power level, caused by a change in operating mode. The RMS current actually reduced from over 4 A to under 3 A, for an increase in real power from 0.54 to 0.59 kW (see Fig. 3*a*). In another case, the RMS current only increased from 4.2 to 4.4 A, for an increase in real power from 0.54 to 0.98 kW (Fig. 3*b*). The Appendix gives a summary of the power quality data for all the heat-pumps, operating near their rated power, in both heating and cooling modes.

3.5 Power factor and displacement power factor

DPF is the cosine of angular difference between fundamental current and voltage, while PF is defined as the ratio of real power to total apparent power (and hence includes harmonics as well as DPF). Therefore

$$\mathrm{PF} = \frac{\text{real power}}{\text{apparent power}} = \frac{\frac{1}{T}\int_0^T \mathrm{vid}\,t}{V_{\mathrm{RMS}} I_{\mathrm{RMS}}} = \frac{\sum_{n=1}^{N} V_n I_n \cos(\phi_n)}{V_{\mathrm{RMS}} I_{\mathrm{RMS}}} \quad (1)$$

If the voltage harmonics are small (as in these tests) then $V_n I_n \cos(\phi_n) \simeq 0$ for $n \neq 1$ and therefore the expression for the

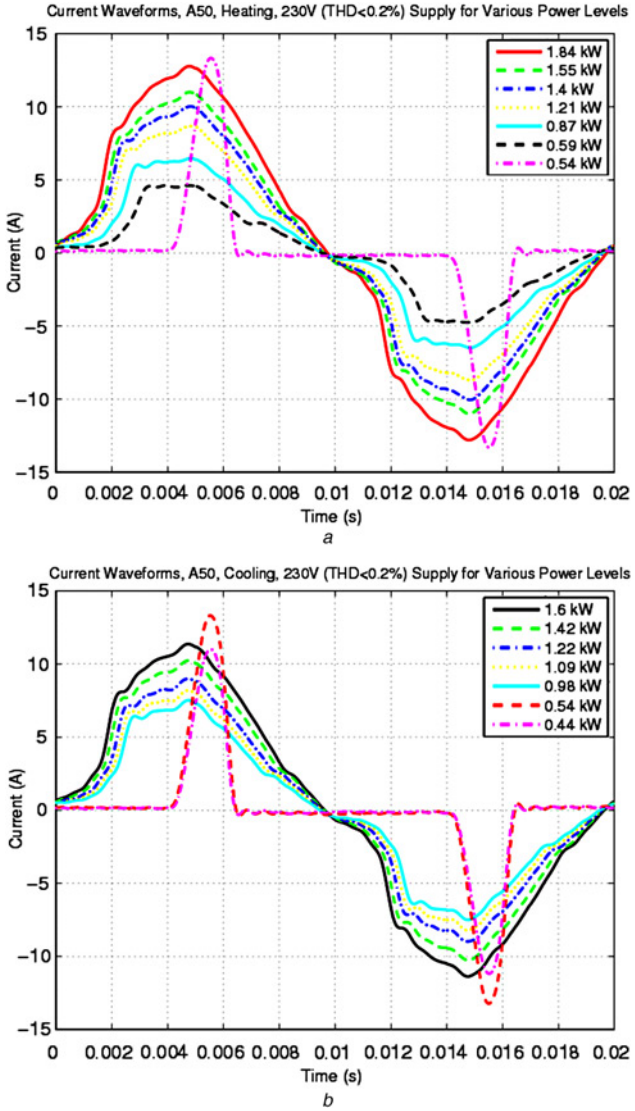


Fig. 3 *Heat-pump A50 current waveforms*
a Heating
b Cooling

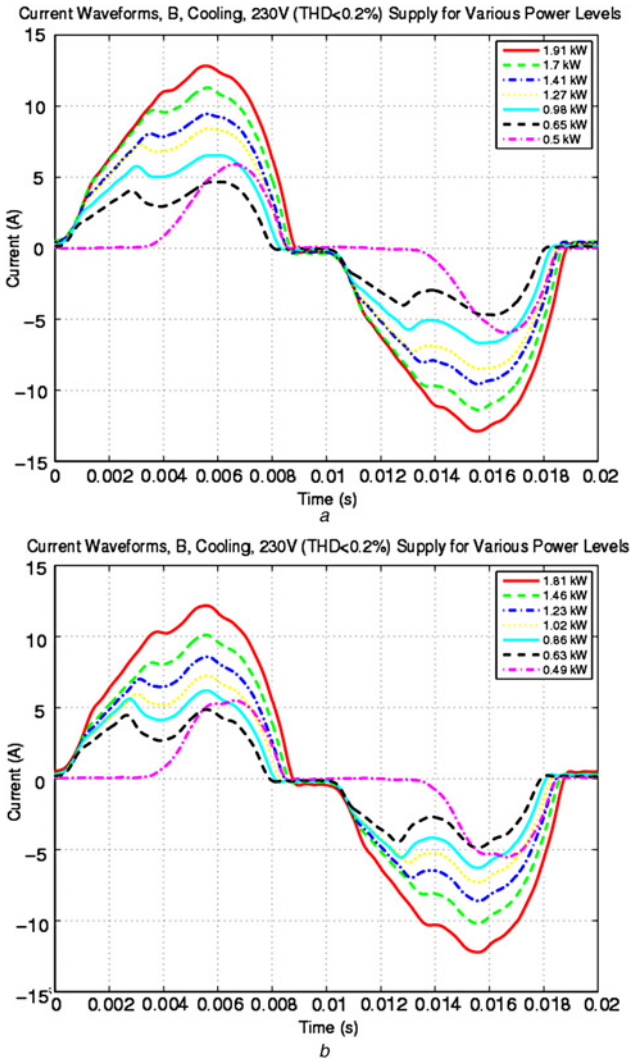


Fig. 4 *Heat-pump B current waveforms*
a Heating
b Cooling

This is an open access article published by the IET under the Creative Commons Attribution-NonCommercial License (http://creativecommons.org/licenses/by-nc/3.0/)

PF can be simplified, with the ratio of RMS fundamental current to RMS total current being expressed as the distortion factor (DF)

$$PF \simeq \frac{V_1 I_1 \cos(\phi_1)}{V_1 I_{\text{RMS}}} = \frac{I_1}{I_{\text{RMS}}} \times \cos(\phi_1)$$
$$= \text{DF} \times \text{DPF} = \frac{\text{DPF}}{\sqrt{1 + \text{THD}^2}} \quad (2)$$

The range of PFs exhibited by all units, under all the operating conditions displayed in Figs. 2–7, varied from 0.55 lagging to 0.93 leading, whereas the range of DPFs varied from 0.88 lagging to 0.97 leading. Although unit *A*50 had the worst PF, its DPF was always close to unity, indicating that the low PF was because of harmonic distortion. The current total harmonic distortion (I_{THD}) levels for unit *A*50 reach 150% of fundamental at low power levels.

The cost of equipment needed to compensate for poor PF, especially for residential customers, who do not have PF limits in their connection agreements, will inevitably be borne by the distribution and transmission networks. There is sometimes a misconception that a low DPF will require PFC capacitors to be installed. This is because of the traditional thinking that loads are predominantly inductive. A low DPF can be because of a leading (rather than lagging) current, as is often the case with modern equipment having an input rectifier with a capacitive DC filter. A low DF will generally require some form of harmonic mitigation.

3.6 *Effect of supply voltage distortion*

The harmonic currents drawn by a heat-pump, as with most other power electronic devices, are influenced by the voltage distortion at the terminals [9]. This voltage distortion may be because of voltage drop across the source impedance caused by its own harmonic currents, as well as the harmonic currents drawn or injected by other non-linear loads or sources connected to the system. To minimise this distortion in the tests, the source was kept as stiff as possible. This is not always a realistic scenario on a typical network, where a V_{THD} of 1–5% of fundamental, or more, is common. In order to show the sensitivity of the results to voltage distortion, three different sources were used to supply heat-pump *D*. They were:

- a relatively high impedance MG set;
- a local mains supply, already distorted by other loads; and
- a stiff programmable source.

Table 2 displays the I_{THD} for heat-pump *D* when supplied from these sources. Of note is the increase in I_{THD} as the terminal

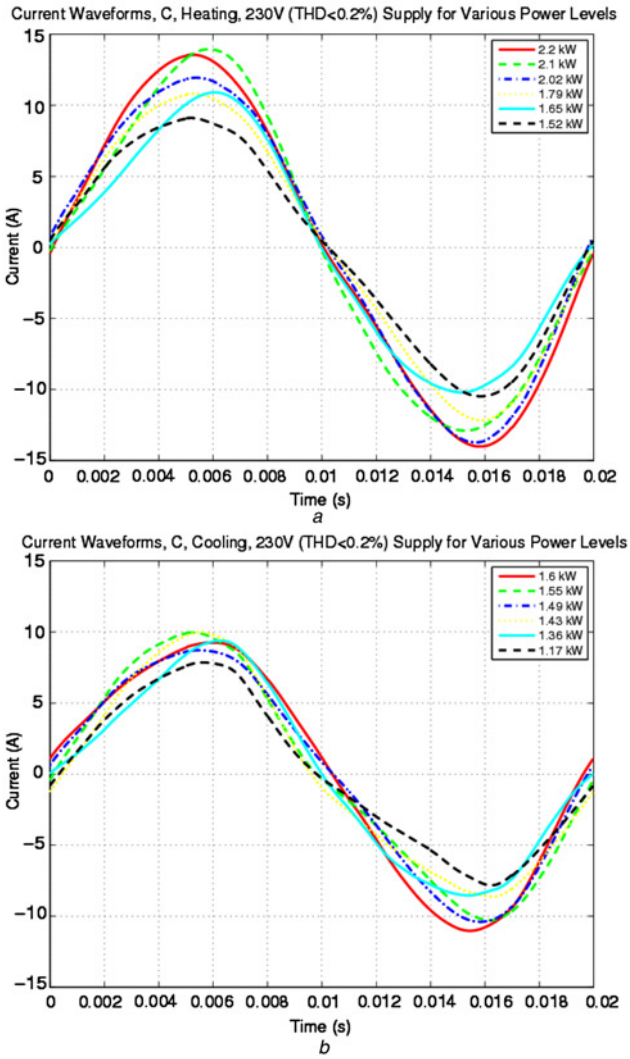


Fig. 5 *Heat-pump C current waveforms*
a Heating
b Cooling

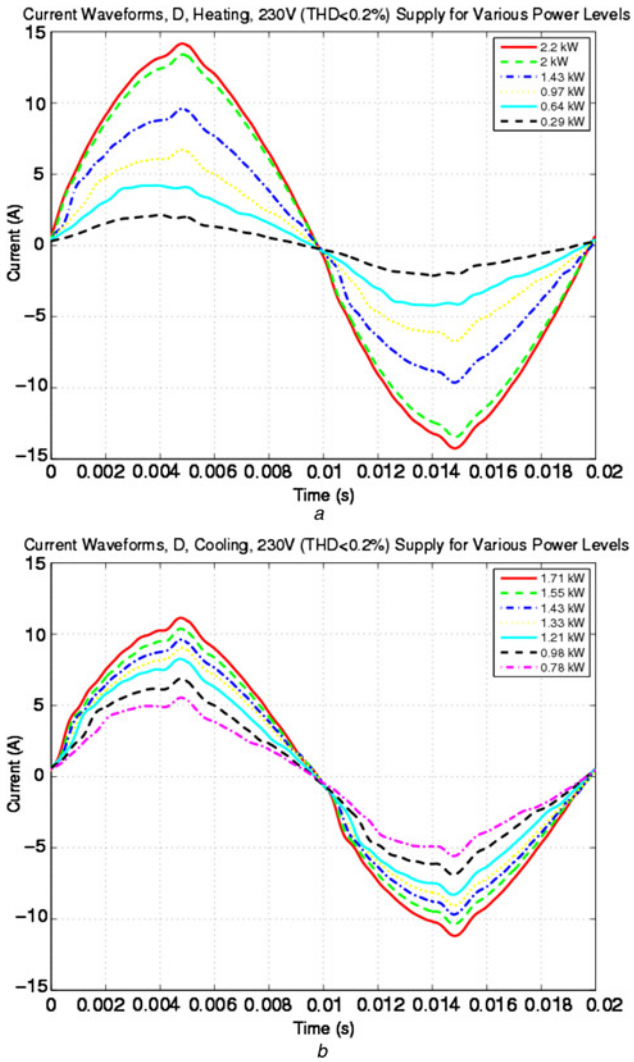


Fig. 6 *Heat-pump D current waveforms*
a Heating
b Cooling

This is an open access article published by the IET under the Creative Commons Attribution-NonCommercial License (http://creativecommons.org/licenses/by-nc/3.0/)

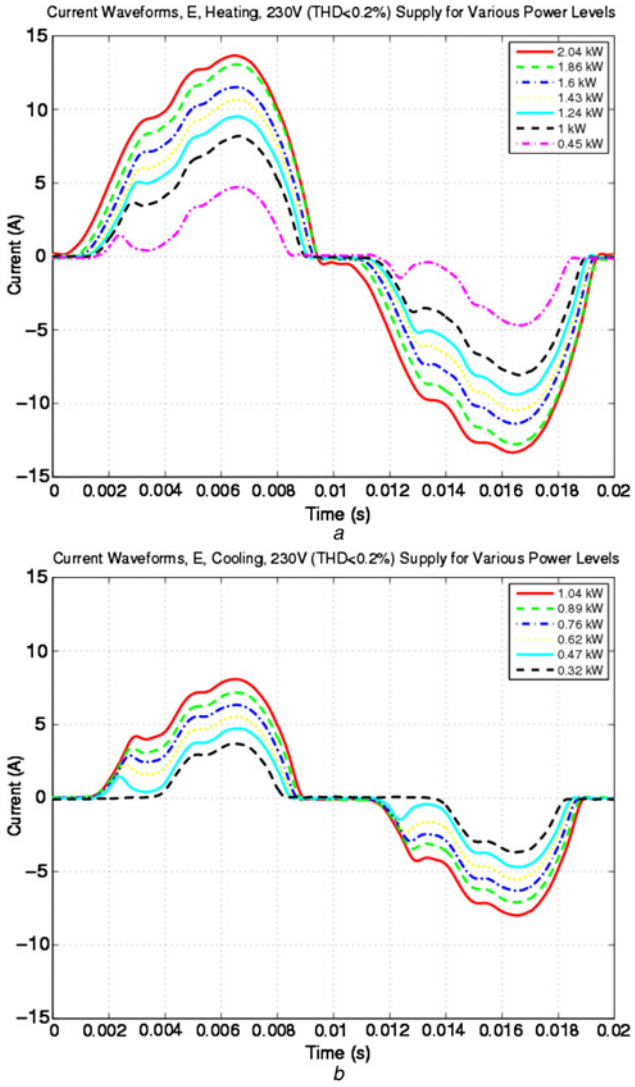


Fig. 7 *Heat-pump E current waveforms*
a Heating
b Cooling

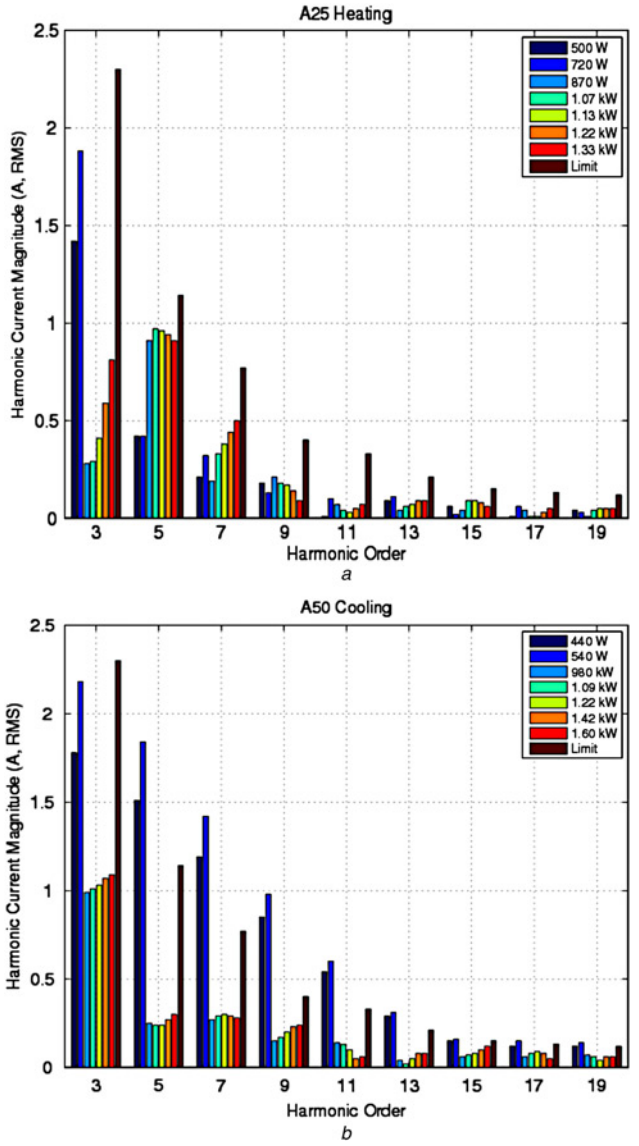


Fig. 8 *Comparison of harmonic current spectra against AS/NZS 61000.3.2*
*a A*25 when heating
*b A*50 when cooling

V_{THD} increases. In order to understand the sensitivity more fully, a tensor representation of the heat-pump is needed, as the heat-pump will exhibit a phase-dependent impedance at harmonic frequencies in the same way as compact fluorescent lamps and HVDC links [10–12].

3.7 *Diversity of harmonics*

The currents of all the inverter-driven heat-pumps running simultaneously in the heating mode, under conditions close to the manufacturers' nominal power levels of Table 1 (similar to the nearest power levels of Figs. 2–7), were summed vectorially. Although only valid for a stiff voltage source, where the current harmonics do not significantly distort the voltage waveform, this nonetheless demonstrates the effect of diversity in the harmonic phase angle. Figs. 9*a* and *b* show compass plots of the third and fifth harmonics (in heating mode), respectively, for the individual inverter-driven heat-pumps as well as the total. The combined total current waveform and its spectrum are displayed in Figs. 9*c* and *d*. Figs. 10*a–d* show that the diversity is slightly worse when in cooling mode. Table 3 shows the I_{THD} for the individual heat-pumps as well as the combined I_{THD} for all the heat-pumps running together. The IEC and AS/NZS standards assume that the diversity factor (α) is 1 for harmonic orders $h < 5$, 1.4 for $5 \leq h \leq 10$ and 2 for $h > 10$. From the measurement results, an actual diversity factor has been calculated, using an iterative procedure, and displayed in Table 4. This shows there is more diversity in the third harmonic than the standards assume, whereas less for all the other harmonic orders. Work on the diversity of harmonics from irrigation pumps has shown a lower diversity than the standards

Table 2 Effect of source (and hence V_{THD}) on I_{THD} for unit *D* (heating)

Voltage source	MG set	Mains supply	Programmable source
voltage *V* RMS	230	231	230
current *A* RMS	10.4	9.9	10.0
real power, kW	2.37	2.24	2.29
apparent power, kVA	2.39	2.28	2.31
reactive power, kVAR	0.25 lead	0.42 lead	0.30 lead
voltage THD, %F	1.8	4.5	0.2
current THD, %F	5.2	6.0	3.8
PF	0.99	0.98	0.99
DPF	1.00	0.99	0.99

This is an open access article published by the IET under the Creative Commons Attribution-NonCommercial License (http://creativecommons.org/licenses/by-nc/3.0/)

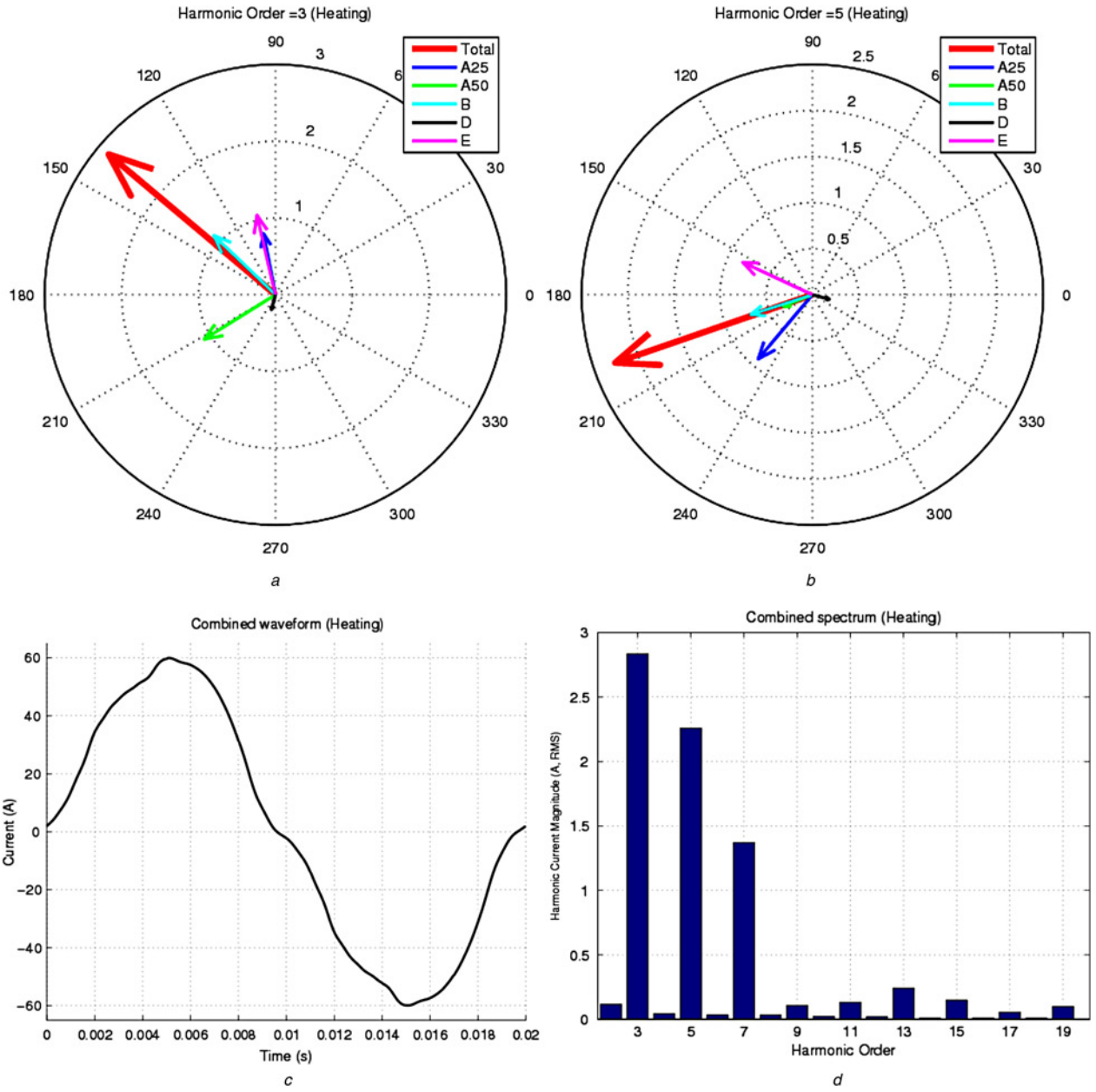


Fig. 9 *Multiple inverter-driven heat-pumps (heating)*
a Compass plot of third harmonic current
b Compass plot of fifth harmonic current
c Combined waveform
d Spectrum of combined waveform

assumed ($\alpha = 1$ at fifth harmonic) [13]. Diversity in household appliances was reported in [14].

4 Heat-pump design

To enable detailed studies of the impact that combinations of heat-pumps will have, a detailed model must be developed. This was achieved by a combination of studying schematic diagrams (where available) and product disassembly, with in-circuit testing techniques. In some cases, particularly in the case of inductive components, parts were removed from PCB assemblies and their parameters measured using appropriate instruments. Schematics of the main power circuits for the five inverter-driven heat-pumps are given in Figs. 11 and 12.

Heat-pumps *A*25, *B* and *E* all employ relatively large lamination steel-cored inductors, in series with a bridge rectifier and DC bus capacitance, to provide shaping of a major lagging current pulse each half-cycle. They also employ a low-frequency switching element which, when activated, causes an additional minor leading current pulse to be drawn each cycle.

Heat-pumps *A*50 and *D* employ much smaller ferrite-cored inductors, in conjunction with a bridge rectifier and a high-frequency switching boost converter.

The inductance values for all inductors were measured (out of circuit) using an HP4192A impedance analyser. The capacitance values were not measured, but the marked nominal value used.

4.1 Heat-pump classification

Based on the performance measurements discussed in Section 3 and the power circuit topologies shown in Figs. 11 and 12, the heat-pumps can be classified as:

This is an open access article published by the IET under the Creative Commons Attribution-NonCommercial License (http://creativecommons.org/licenses/by-nc/3.0/)

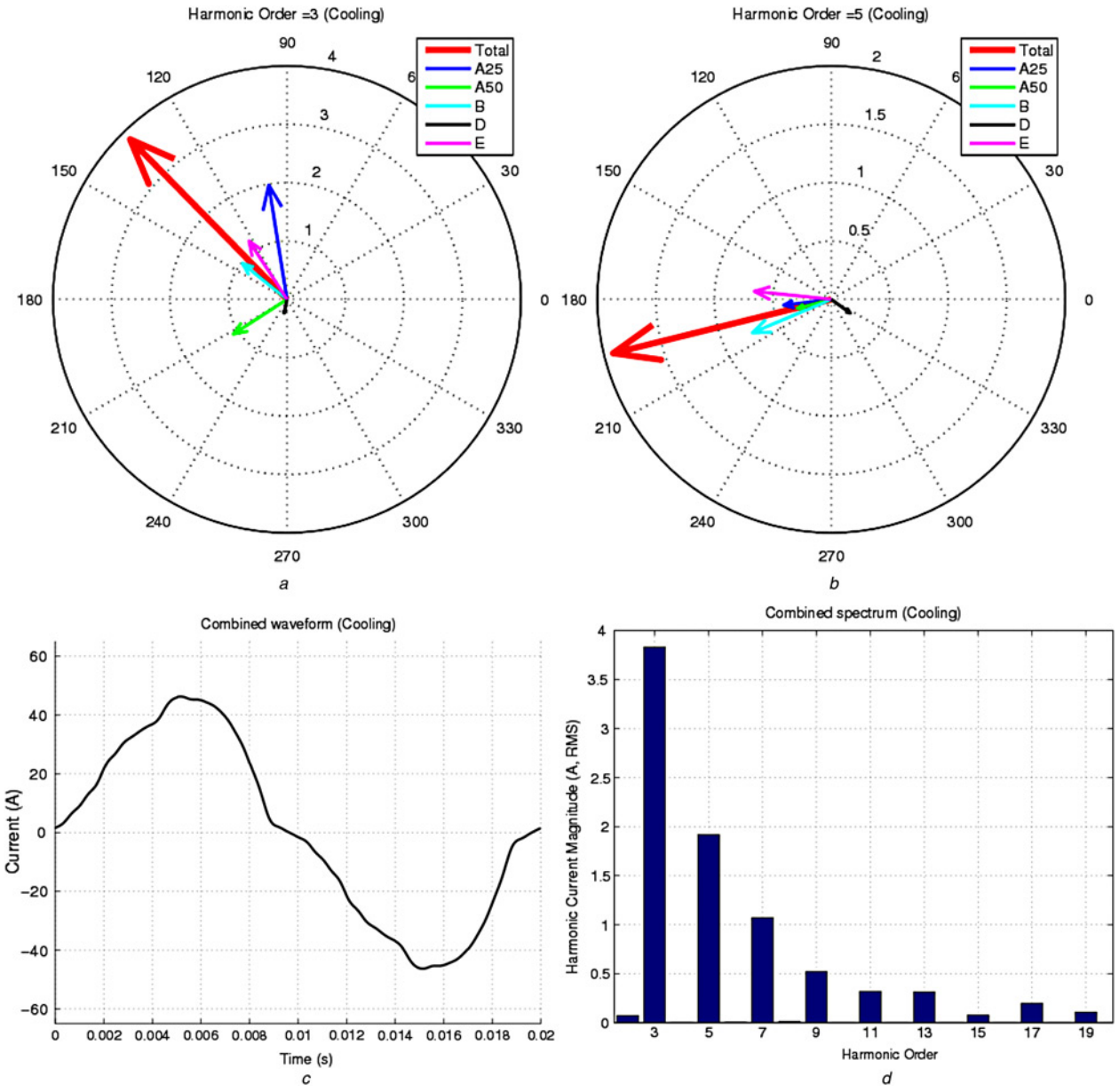


Fig. 10 *Multiple inverter-driven heat-pumps (cooling)*
a Compass plot of third harmonic current
b Compass plot of fifth harmonic current
c Combined waveform
d Spectrum of combined waveform

Table 3 I_{THD} of individual heat-pumps and their combination when running together

Heat-pump	Heating		Cooling	
	THD, % fundamental	I_1, Amps	THD, % fundamental	I_1, Amps
*A*25	22.99	5.78	55.40	3.72
*A*50	15.09	8.04	17.24	7.00
B	17.00	8.32	16.73	7.89
D	3.32	9.52	5.32	7.36
E	16.35	8.95	30.74	4.60
all heat-pumps	9.64	40.44	14.97	29.96

Table 4 Calculated diversity factor (α)

Harmonic order	Heating	Cooling
3	1.393	1.318
5	1.250	1.137
7	1.190	1.170
11	—[a]	1.430
13	1.200	1.100
17	—[a]	1.120
19	1.720	1.465
23	1.540	1.340
25	1.465	1.200
29	1.460	1.680
31	1.045	1.130

[a]No solution found.

This is an open access article published by the IET under the Creative Commons Attribution-NonCommercial License (http://creativecommons.org/licenses/by-nc/3.0/)

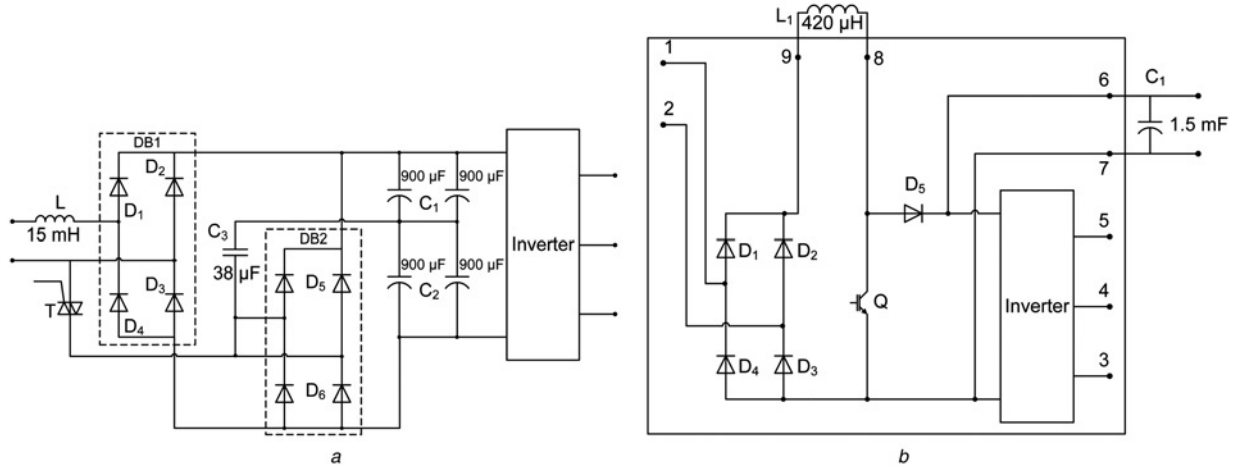


Fig. 11 *Schematics of the main power circuits for heat-pumps A25 and A50*
a Schematic of heat-pump *A25*
b Schematic of heat-pump *A50*

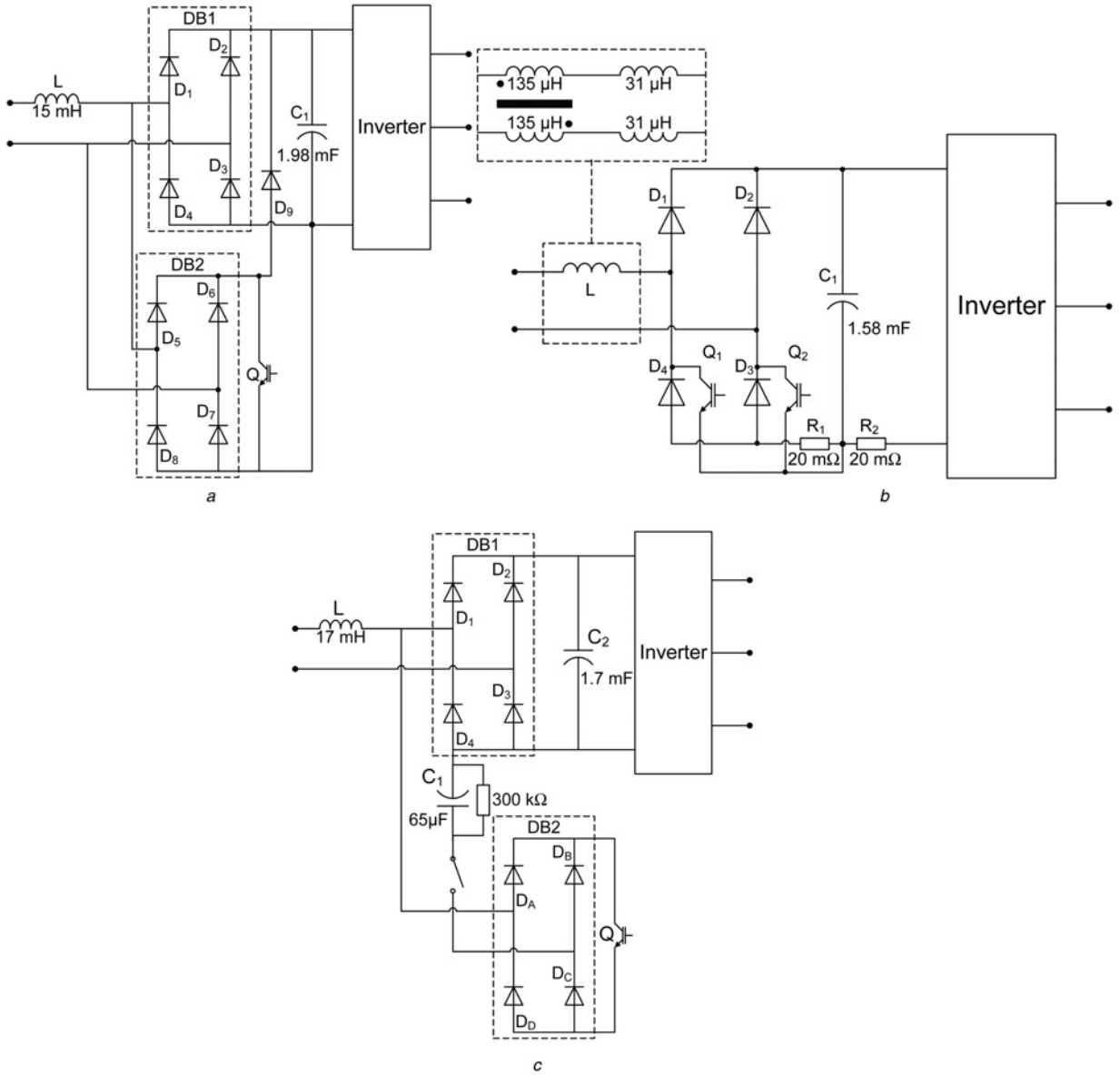


Fig. 12 *Schematics of the main power circuits for heat-pumps B, D and E*
a Schematic of heat-pump *B*
b Schematic of heat-pump *D*
c Schematic of heat-pump *E*

This is an open access article published by the IET under the Creative Commons Attribution-NonCommercial License (http://creativecommons.org/licenses/by-nc/3.0/)

doi: 10.1049/joe.2013.0012

- Non-inverter heat-pump (C) which always exhibits reasonably high, lagging PF and DPF and low I_{THD}.
- Type 1*a* inverter units ($A25$ and B), which exhibit relatively low, lagging DPF and very low, lagging PF at lower power levels, changing abruptly to higher, leading PF and DPF at higher power levels.
- Type 1*b* inverter unit (E), which exhibits relatively low, lagging DPF and low, lagging PF at lower power levels, improving, but remaining lagging, as power level increases.
- Type 2 inverter unit ($A50$), which exhibits extremely low, lagging PF at lower power levels, changing abruptly to much higher, leading PF at higher power levels, although the DPF remains close to unity at all levels.
- Type 3 inverter unit (D), which exhibits high, leading PF and DPF throughout its operating range.

This classification is shown diagrammatically in Fig. 13.

4.2 *Low-frequency switching circuits*

Heat-pump $A25$ (Fig. 11*a*) employs a Triac (T) to switch a relatively small, non-polarised capacitor, C_3, into the circuit shortly after the voltage zero-crossing. On the positive half-cycle C_3 charges through L, D_1, C_1 and T to half the DC bus voltage (producing the minor leading current pulse shown in Fig. 2), at which point D_3 turns on such that C_1 and C_2 charge in series through L, D_1 and D_3, producing the major lagging current pulse. On the negative half-cycle C_3 charges through L, D_4, C_2 and T to half the DC bus voltage with the opposite polarity, at which point D_2 turns on such that C_1 and C_2 charge in series through L, D_2 and D_4. Operation is hence entirely symmetrical.

Heat-pump B (Fig. 12*a*) employs a second bridge rectifier, shunted by an insulated gate bipolar transistor (IGBT) (Q) and in series with a catch diode (D_9) to form a boost converter, in parallel with the main rectifier. A low-frequency pulse train (at about 4 kHz) applied to the gate of the IGBT, shortly after the zero-crossing, allows a minor leading current pulse (shown in Fig. 4) to be shaped, followed by the major lagging pulse through the main rectifier.

Heat-pump E (Fig. 12*c*) also employs a second bridge rectifier, shunted by an IGBT (Q), but this time in series with a small capacitor, C_1 (and a relay contact allowing the whole circuit to be switched out). Unlike the other circuits, operation is not entirely symmetrical on opposite half-cycles. Assuming the relay is closed, on the positive half-cycle Q is turned on shortly after the voltage zero-crossing, causing C_1 to charge through L, D_A, Q, D_C and D_3. When C_1 voltage reaches the DC bus voltage (or when Q is turned off before then) D_1 turns on and the current flows through L, D_1, C_2 and D_3 in series. On the negative half-cycle, Q is turned on shortly after the voltage zero-crossing causing C_1 to discharge through C_2, L, D_D, Q, D_B and D_2. When C_1 voltage reaches zero (or when Q is turned off before then) D_4 turns on and the current flows through L, D_4, C_2 and D_2 in series. Thus C_1 can be a polarised electrolytic type and a split DC bus (as with unit $A25$) is not needed. (C_1 is shunted by a bleed resistor as shown). The circuit operation described causes the minor leading current pulse (C_1 in circuit), followed by the major lagging pulse (C_1 out of circuit) shown in Fig. 7.

All three converters ($A25$, B and E) have a steel-cored inductor of similar electrical size (15–17 mH), although unit $A25$'s is physically smaller, because of the lower power, and hence peak current, rating.

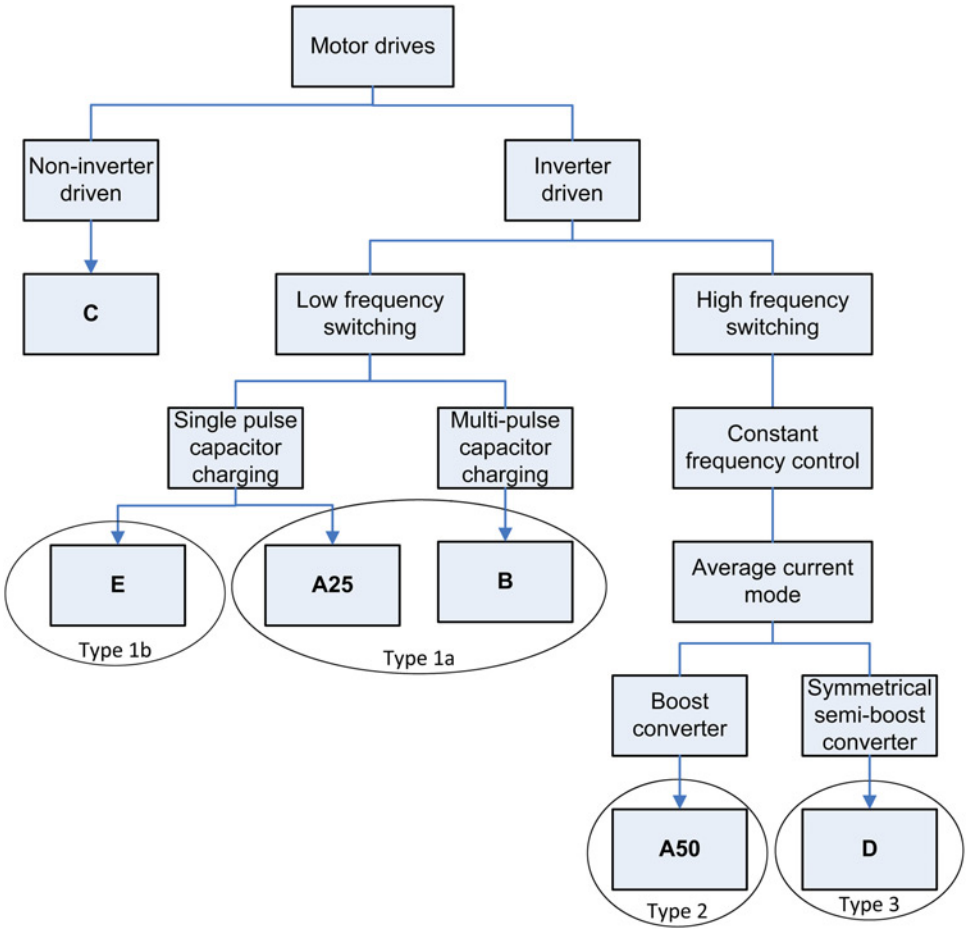


Fig. 13 *Classification of heat-pumps, based on PFC rectifier type*

This is an open access article published by the IET under the Creative Commons Attribution-NonCommercial License (http://creativecommons.org/licenses/by-nc/3.0/)

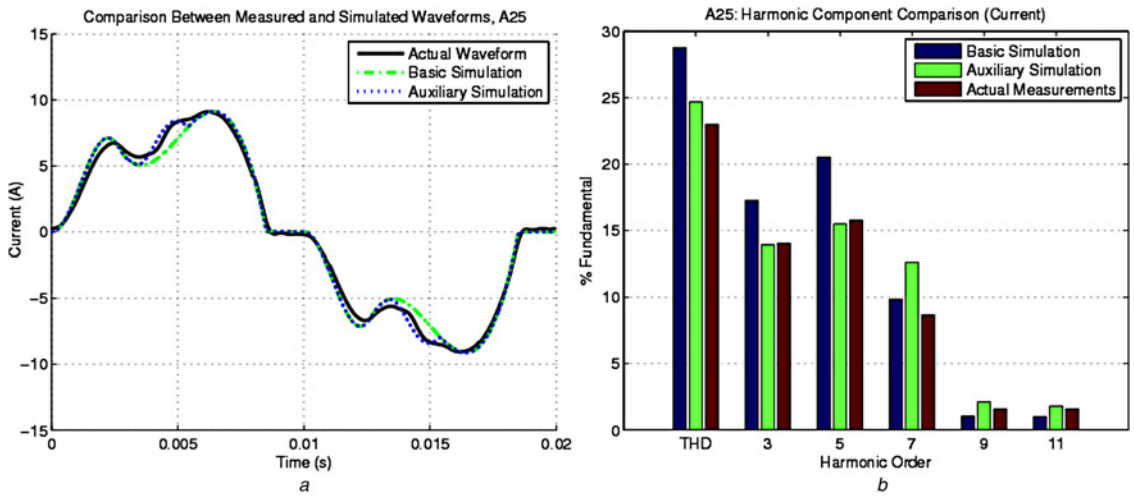


Fig. 14 *Waveform and spectrum comparisons for unit A25*
a Current waveforms and heat-pump *A*25
b Harmonic spectra and heat-pump *A*25

4.3 High-frequency switching circuits

Heat-pump *A*50 (Fig. 11*b*) employs a conventional PWM boost topology, switching at 28.8 kHz with an IGBT (*Q*). From the waveforms of Fig. 3, it can be seen that, under some conditions, the IGBT does not switch at all, the 420 µH ferrite-cored inductor serving only to make the high CF current lag slightly, rather than lead.

Heat-pump *D* (Fig. 12*b*) employs a symmetrical PWM semi-boost converter [15] using IGBTs (Q_1 and Q_2). The symmetry extends to the inductor, which takes the form of a coupled choke symmetrically placed in both live and neutral conductors. Measurements on the ferrite-cored inductor reveal self-inductance of 166 µH for each winding, mutual inductance of 135 µH and hence effective differential mode inductance of about 600 µH. Current-sensing resistors for both the PFC rectifier and the inverter are shown.

Measurements indicate that both these converters (*A*50 and *D*) are operating under constant frequency, average current mode control [16, 17]. Both of these converters also have substantial additional differential and common mode (CM) filter components which are not shown in Figs. 11*b* and 12*b*.

Note that all the heat-pumps have effective DC bus capacitance in the range 1.5–2 mF, except for *A*25, which has 900 µF, but is only rated for about half the power of the others.

4.4 Observations on design, based on measurements

At lower power levels units *A*25, *B* and *E* do not make use of their auxiliary current shaping circuit, only switching it in above approximately 800, 500 and 400 W, respectively. Fig. 2 shows that the leading current pulse for unit *A*25 has the same magnitude and duration regardless of power level. This is because, once triggered, the Triac switch cannot be turned off until the next zero-crossing; hence the pulse is determined by *L* and C_3 (Fig. 11*a*). This explains the jump from lagging to leading PF especially apparent just above 800 W. The firing angle after zero-crossing for the Triac could be altered, but this does not seem to occur with the simple control scheme implemented.

The measurement results for heat-pump B (shown in Fig. 4) demonstrate that the number and duration of IGBT switchings can be used to control both the amplitude and the timing of the leading current pulse. Closer inspection shows that at a short fixed time after each zero-crossing there is a period of relatively high di/dt (fixed for all power levels) when *Q* is on (Fig. 12*a*), followed by a period of controlled constant di/dt (higher for higher power levels) achieved by low-frequency modulation of the IGBT. During *Q*'s off-time some of the inductor energy is released to the DC bus. It would appear that the modulation scheme could be readily altered to give a slightly less leading full-load current with this circuit.

The results for unit *E* (shown in Fig. 7) demonstrate that a single turn-on of *Q* (Fig. 12*c*) occurs each half-cycle, with both turn-on instant and pulse duration variable, depending on power level. An earlier turn-on instant, or a larger value for C_1, might result in a slightly less lagging full-load current.

Heat-pumps *A*50 and *D* are both theoretically capable of achieving high PF and low distortion at all power levels. Unit *D* does indeed perform well at all power levels; however the boost switch of heat-pump *A*50 (*Q* in Fig. 11*b*) is disabled at lower power levels, resulting in distortion exceeding the limits specified in the standard. Although some small power savings may result from not running the high-frequency boost circuit, there will be additional losses in the inductor because of high RMS current; hence it is unclear why the manufacturer has implemented this behaviour.

5 Simulations and verification

5.1 PSCAD/EMTDC models

The development of simulation models for the heat-pumps is desirable for two reasons. Firstly it provides confirmation that the individual circuit operation is correctly understood, and secondly it allows the effect of many heat-pumps on any network to be assessed. Each model consists of a power stage, based closely on the circuits determined previously (Figs. 11 and 12), and a control stage, synthesised to give close agreement with the observed real-world waveforms. In all cases the inverter, loaded by the three-phase compressor, is modelled by a constant power load, represented by a DC voltage source shunted by a resistor.

5.1.1 Low-frequency switching circuits: To model heat-pump *A*25 a pair of anti-parallel thyristors is used, to simulate the triac of the real circuit. A voltage controlled oscillator (VCO) is used as a sawtooth generator, synchronised to the mains source, which provides a signal ramping between 0 and 360°. This is compared with a constant (but adjustable) firing angle α (between 0 and 180°) for the positive half-cycle and $(\alpha + 180)°$ for the negative cycle, to produce the thyristor gate pulses. Both α and the constant power load parameters can be adjusted to match the simulated input current waveform to the real-world measurements.

This is an open access article published by the IET under the Creative Commons Attribution-NonCommercial License (http://creativecommons.org/licenses/by-nc/3.0/)

In the model for heat-pump *B*, the IGBT, on which the boost converter is based, is driven by a pulse train synthesised from a single long pulse followed by several further pulses, at around 4 kHz, with pulse width reducing as the mains voltage rises, to mimic the observed two-slope, real-world current rise. The actual pulse widths can be adjusted, as can the constant power load parameters, to give the closest match between the simulated input current waveform and the real-world measurements.

In the model of heat-pump *E*, apart from the load resistance and DC bus voltage, there are two variables that can be set for the model: time delay after voltage zero-crossing for 100 Hz IGBT turn-on pulse (t_d) and duration of IGBT turn-on pulse (t_p). The DC bus voltage is set to the real-world measured value, when operating at a certain power level, and the load resistance is set to give the relevant real power; t_d and t_p are then set to give the closest match between the simulated and the measured input current waveforms.

5.1.2 High-frequency switching circuits: With the high-frequency switching types *A*50 and *D* there is considerable high-frequency ripple current present in the inductor, so the input filters employed also have to be modelled to obtain simulation results close to the real-world observed input current waveforms.

Although the power circuit topologies are different, both the high-frequency switching circuits were modelled with a similar design of average current mode controller. A bipolar sawtooth signal is produced by a VCO, at the relevant observed switching frequency, to which amplitude and offset adjustments can be made. The modified sawtooth is fed into input B of a PWM comparator. Input A of the comparator is fed by a signal derived from the error between the inductor current, I_{out}, and a reference current, I_{ref}, which in turn is derived from the input voltage waveform. The actual error signal is first passed through a proportional-integral (PI) control element, with adjustable proportional gain and integral time constant, to obtain the input *A* signal.

In the model for heat-pump *A*50, each IGBT switching cycle is initiated by the fixed frequency (28.8 kHz) clock pulse, which is synchronised to the reference sawtooth, and is terminated by the high-going output of the PWM comparator. The offset adjustment for the sawtooth is positive, resulting in positive di/dt, but negative d^2i/dt^2, just after each zero-crossing, as observed in the real-world measurements. The sawtooth amplitude adjustment, the proportional gain and integral time constant of the PI controller, the reference current and, of course, the constant power load are all adjusted to attempt to match the simulated input current waveform to the real-world measurements.

In the model for heat-pump *D*, on the positive half-cycle each Q_1 switching cycle is initiated by the fixed frequency (23.8 kHz) clock pulse, synchronised to the reference sawtooth and is terminated by the high-going output of the PWM comparator. On the negative half-cycle Q_1 is disabled and Q_2 is switched in a similar fashion.

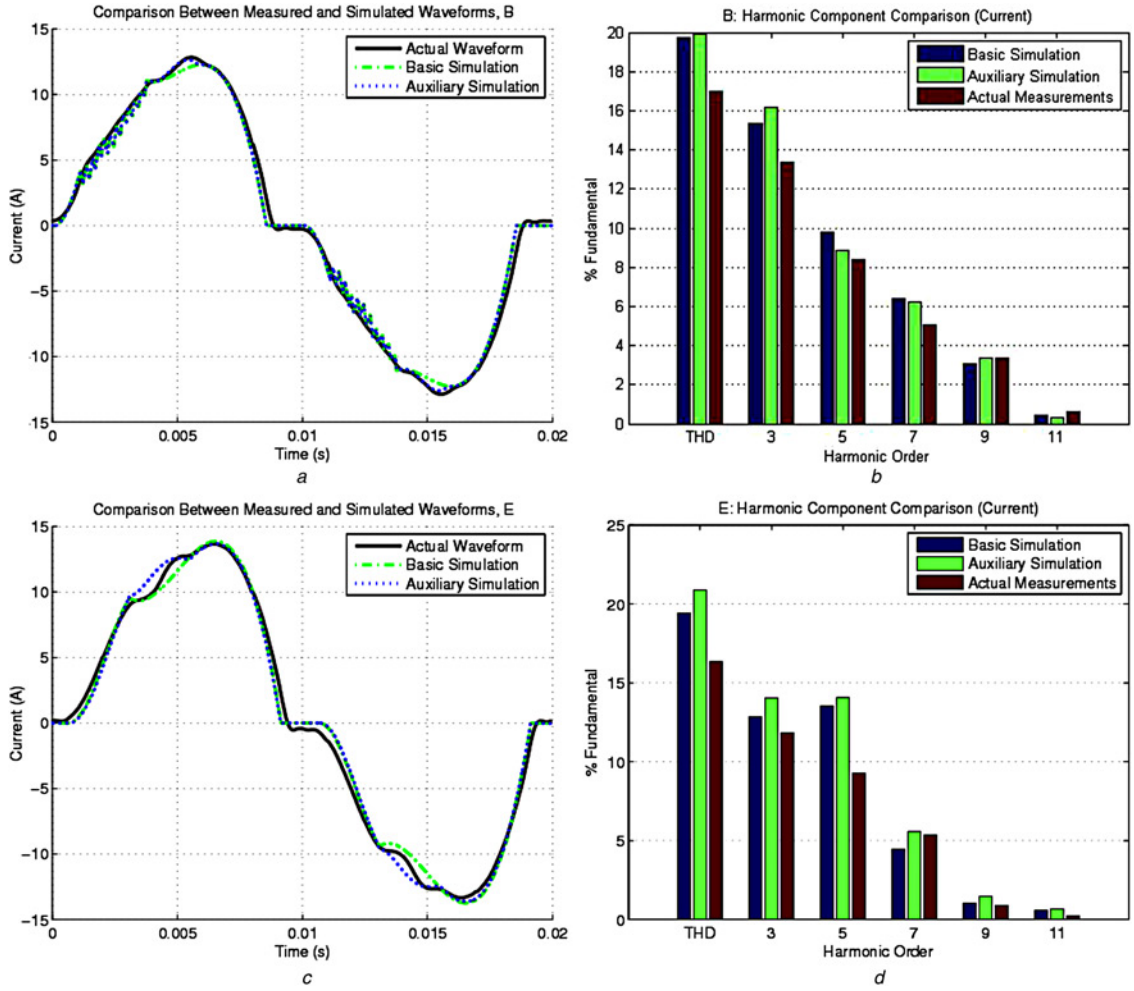


Fig. 15 *Waveform and spectrum comparisons for units B and E*
a Current waveforms and heat-pump *B*
b Harmonic spectra and heat-pump *B*
c Current waveforms and heat-pump *E*
d Harmonic spectra and heat-pump i

doi: 10.1049/joe.2013.0012
This is an open access article published by the IET under the Creative Commons Attribution-NonCommercial License (http://creativecommons.org/licenses/by-nc/3.0/)

The offset adjustment for the sawtooth is negative, resulting in positive di/dt and positive d^2i/dt^2, just after each zero-crossing, as observed in the real-world measurements. The sawtooth amplitude adjustment, the proportional gain and integral time constant of the PI controller, the reference current and the constant power load can be adjusted in order to improve the match with the laboratory measurements. Again the DC bus voltage and load resistance are set to give the measured real-world values and the adjustable parameters are set to give a close match between the simulated and the measured input current waveforms.

5.2 *Verification*

Each of the five simulation models was run at the highest measured power levels, with a run time of ten mains cycles to allow settling to steady-state. The simulated voltage source is perfect, with zero source impedance. The measured and simulated results, shown as 'basic simulation' are compared in Figs. 14–16, which show the current waveforms and harmonic spectra.

The correlation is reasonably good for most harmonics for most of the models, although third and fifth are significantly different for heat-pump *D*, and fifth for unit *E*, in percentage terms. The 'basic simulation' waveforms are generally in reasonably good agreement with the measurements. However, some discrepancies can be noted:

- With the single pulse current shaping types (*A*25 and *E*) the exact turn-on instant of Triac or IGBT, and the actual value of the small capacitor (nominally 38 and 65 μF, respectively), affect the shape of the leading portion of the current waveform.
- There is additional electromagnetic compatibility (EMC) filtering on the multiple-pulse current shaping type (*B*) which is not included in the model, accounting for the 4 kHz ripple visible only in the simulation.
- Each heat-pump also has auxiliary power circuits, such as local power supply and fan drives, supplied from a separate capacitor-filtered bridge rectifier, accounting for the additional current drawn for a short period around the peak and trough of the supply voltage waveform.

In order to improve correlation, an attempt was made to add a representation of the auxiliary power circuits to the models (labelled 'auxiliary simulation'). A bridge rectifier across the mains supply, with an LC filter and a load resistance on the DC side, was added to each model, with values as given in Table 5. Component values were identified to give the best time domain fit to the 'missing' portion of the 'basic simulation' waveforms. Correlation between measured and modelled results is generally improved, especially for units *A*25, *A*50, *B* and *D*. Frequency domain results for units *B* and *E* are neither significantly better nor worse than in the 'basic simulation' case, although the time domain results certainly look more accurate (especially for unit *B*). Remaining discrepancies are likely to be at least partially caused by one or more of the following:

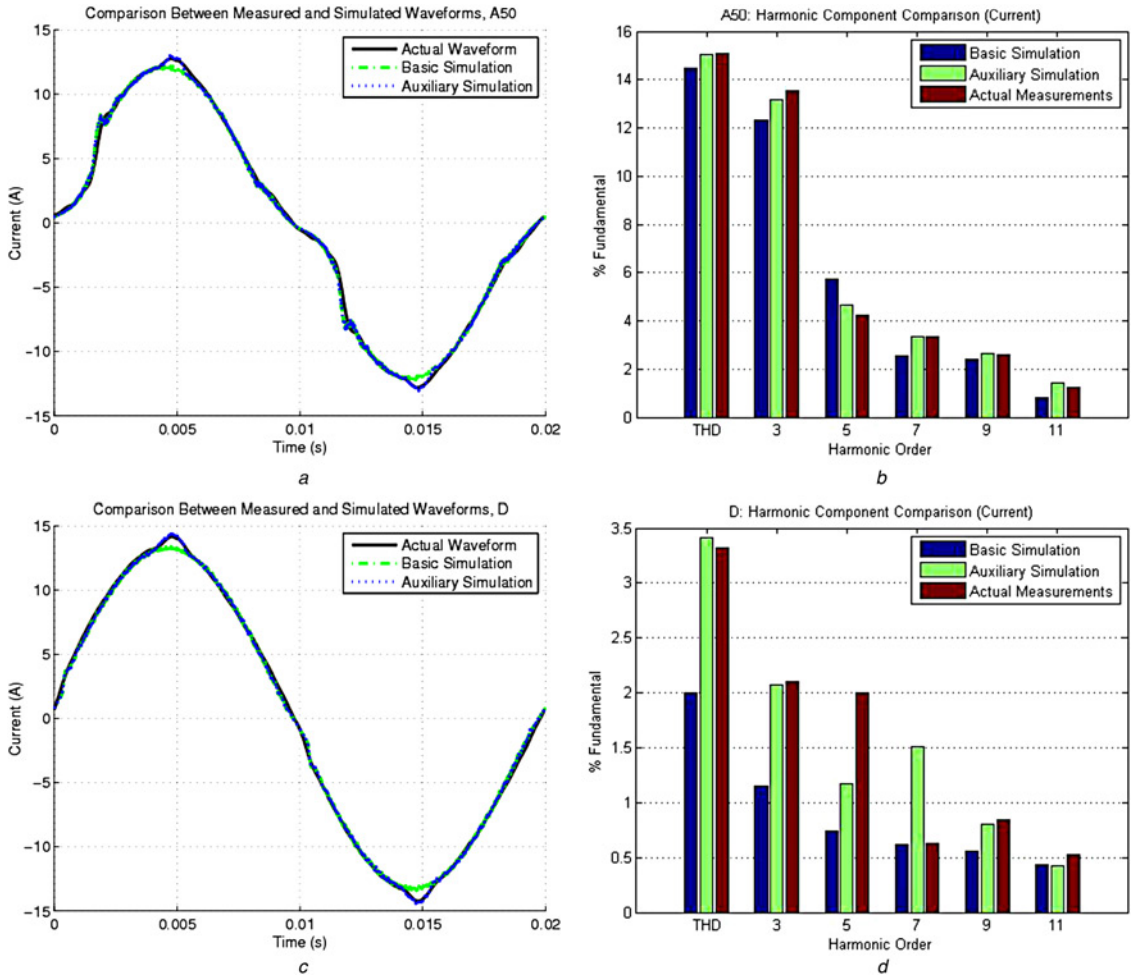


Fig. 16 *Waveform and spectrum comparisons for units A50 and D*
a Current waveforms and heat-pump *A*50
b Harmonic spectra and heat-pump *A*50
c Current waveforms and heat-pump *D*
d Harmonic spectra and heat-pump *D*

This is an open access article published by the IET under the Creative Commons Attribution-NonCommercial License (http://creativecommons.org/licenses/by-nc/3.0/)

Table 5 Auxiliary power circuit model component values

	*A*25	*B*	*E*	i50	*D*
L, mH	25	10	10	4	5
C, μF	15	39	22	25	25
R, Ω	1170	4650	2000	5000	3500

Table 6 Heat-pump retail prices and power circuit component costs

Type	Retail price, NZ$	Heating capacity, kW	Retail price, NZ$/kW	Component cost, US$/kW
*A*25	1116	3.4	328	29
B	2041	6.25	327	17
E	1512	5.5	275	20
*A*50	1575	5.8	272	12
D	1687	5.6	301	19
C	900	5.6	161	1.5

- The models do not incorporate effective series resistance (copper and core losses), or *B*–*H* characteristics, of inductive components.
- The models are using nominal, not measured, capacitance values.
- Some heat-pumps have more than one auxiliary power circuit, and filters used on auxiliary power circuits may be of higher order than the simple RLC assumed.

5.3 *Discussion regarding choice of PFC rectifier topology*

In order to attempt to understand the drivers for different designs, a cost estimate of the PFC rectifier implementations was undertaken. This was to give a relative, rather than an absolute, indication of power circuit cost. Table 6 gives the pertinent results from this, such as heat-pump retail price in NZ$ / kW of nominal heating capacity and power circuitry component cost price in US$ / kW of nominal heating capacity. Competitive prices for the main power circuit (as per Figs. 11 and 12) components (at 1000 + volume) were obtained. Inductive components tend to be custom made and their costs were estimated by choosing the closest standard core (and where applicable, coil-former) and an estimated cost of winding, again at 1000 + volume. The control circuit, printed circuit board and assembly costs were neglected. The power circuit of unit C consists only of a 50 μF motor run capacitor (contactor-relay not included).

All five inverter-driven types have comparable price per kW. The smallest unit (*A*25) is marginally the most expensive per kW and has the highest per kW power circuit component cost, largely because of the multiple bus capacitors used. *A*50 has the lowest power circuit component cost, mainly because of having the smallest main inductor (electrically and physically) and only a single CM choke (as opposed to three CM chokes for the other high-frequency switching heat-pump, *D*). Since cost is not a major factor in the choice of topology, other reasons, such as heat-pump designers' lack of familiarity with high-frequency power electronics topologies, their associated control strategies and EMC challenges, may be responsible.

6 Conclusions and further work

The harmonic performance of several commonly used inverter-driven heat-pumps has been reported, showing a diversity of characteristics (classified as Type 1*a*, 1*b*, 2 or 3), as compared with a directly connected induction motor unit. These characteristics have been traced back to the rectifier power circuit design of the heat-pumps, with the operation verified by comparing simulation results with actual measurements. This now allows 'what if' studies to be performed using the models created. It also shows the wisdom of deploying a variety of heat-pumps in the same street, to achieve harmonic diversity, rather than committing to a single preferred supplier.

At lower input power levels, some of the inverter-driven heat-pumps produce high harmonic current levels. This is because three of the five heat-pumps concerned (*A*25, *B* and *E*) do not use their auxiliary current shaping circuit at low power levels. Although the harmonic levels are high, the device may technically comply with AS/NZS 61000.3.2, as annex C.12 indicates that the appliance is operated with the rated input power for compliance testing. This is of concern, as many units may be simultaneously operating at low-power levels. The CCFs of some of the heat-pumps can be very high at lower power levels, resulting in a very high peak current, which is undesirable. Only the Type 3 inverter-driven heat-pump (unit *D*) exhibits low-current distortion over a wide operating range.

The PF of the non-inverter-driven heat-pump is always reasonably high and lagging. The PF of the Type 1 inverter-driven units is reasonably high (leading for 1*a* and lagging for 1*b*) near the rated power. Below rated power the PF is low and lagging, even when the power drawn is an appreciable percentage of the rated power. The Type 2 unit's PF is high and leading near the rated power. At lower power levels it is very low and lagging. The Type 3 inverter drive unit has a PF that is always high and leading.

Although the heat-pumps are rated for a given input power on their energy efficiency labels, this is not a good guide for assessing their maximum power consumption, which may be significantly higher. For example, unit *A*25 has a rated input power of 0.83 kW, while these tests have shown that it can draw up to 1.33 kW on occasions.

7 Acknowledgments

The financial support for this research from Transpower New Zealand Ltd., the New Zealand Electricity Engineers' Association and the New Zealand Foundation for Research in Science and Technology (now MBIE) is gratefully acknowledged. The authors would also like to thank Ken Smart (University of Canterbury) and Stewart Hardie and Dudley Smart (Electric Power Engineering Centre) for their help.

8 References

[1] French L.: 'Active cooling and heat-pump use in New Zealand – survey results'. BRANZ Study, Report No. 186, 2008
[2] Goetzler W., Zogg R., Lisle H., Burgos J.: 'Ground-source heat-pumps: overview of market status, barriers to adoption, and options for overcoming barriers'. Report for US Department of Energy, Navigant Consulting, February 2009
[3] IEC 61000-3-2: Title: Electromagnetic compatibility (EMC) – part 3–2: limits – limits for harmonic current emissions (equipment input current ≤16 A per phase)
[4] AS/NZS 61000.3.2:2007, 'Electromagnetic compatibility, part 3.2: limits–limits for harmonic current emissions', Standards Australia/Standards NZ
[5] Mohan N.: 'Electric drives: an integrative approach' (MNPERE, Minneapolis, 2000), ISBN 0-9663530-1-3
[6] Jungreis A.M., Kelley A.W.: 'Adjustable speed drive for residential applications', *IEEE Trans. Ind. Appl.*, 1995, **31**, (6), pp. 1315–1322
[7] Domijan A., Hancock O., Maytrott C.: 'A study and evaluation of power electronic based adjustable speed motor drives for air conditioners and heat-pumps with an example utility case study of the Florida power and light company', *IEEE Trans. Energy Convers.*, 1992, **7**, (3), pp. 396–404
[8] AS/NZS 3823.1.1:1998, 'Performance of electrical appliances – air conditioners and heat-pumps', Standards Australia/Standards NZ
[9] Arrillaga J., Watson N.R.: 'Power system harmonics' (John Wiley & Sons, West Sussex, 2003, 2nd edn.)

This is an open access article published by the IET under the Creative Commons Attribution-NonCommercial License (http://creativecommons.org/licenses/by-nc/3.0/)

[10] Watson N.R., Scott T., Hirsch S.: 'Implications for distribution networks of high penetration of compact fluorescent lamps', *IEEE Trans. Power Deliv.*, 2009, **24**, (3), pp. 1521–1528
[11] Wei Z., Watson N.R., Frater L.P.: 'Modelling of compact fluorescent lamps'. Proc. 13th Int. Conf. Harmonics and Quality of Power Quality (ICHQP 2008), September–October 2008
[12] Smith B.C., Watson N.R., Wood A.R., Arrillaga J.: 'Harmonic tensor linearisation of HVdc converters', *IEEE Trans. Power Deliv.*, 1998, **13**, (4), pp. 1244–1250
[13] Watson N.R., Hardie S., Scott T., Hirsch S.: 'Improving rural power quality in New Zealand'. EEA Conf., 17–18 June 2010
[14] Hardie S., Watson N.R.: 'The effect of new residential appliances on power quality'. Australasian Universities Power Engineering Conf. (AUPEC) 2010, 5–8 December 2010
[15] Singh B., Singh B.N., Chandra A., Al-Haddad K., Pandey A., Kothari D.P.: 'A review of single-phase improved power quality AC-DC converters', *IEEE Trans. Ind. Electron.*, 2003, **50**, (5), pp. 962–981
[16] Dixon L.: 'Average current mode control of switching power supplies'. Unitrode Power Supply Design Seminar Manual, SEM-700, Unitrode, 1990
[17] Dixon L.: 'High power preregulators for off-line power supplies'. Unitrode Power Supply Design Seminar Manual, SEM-600A, Unitrode, 1988

9 Appendix

See Tables 7 and 8

Table 7 Comparison of power quality, near rated power and heating

Type	P_{nom}, kW	*i*, kW	*S*, kVA	*Q*, kVAr	I_{THD}, %fund.	CF	PF	DPF
*A*25	0.83	0.72	0.92	0.36 lag	56.5	1.97	0.78	0.89
		0.87	0.93	0.25 lead	25.7	1.60	0.93	0.96
*A*50	1.6	1.55	1.58	0.17 lead	17.5	1.60	0.98	0.99
B	1.73	1.70	1.72	0.12 lead	17.2	1.51	0.98	1.00
C	1.90	1.79	1.81	0.15 lag	10.3	1.45	0.99	1.00
		2.02	2.05	0.15 lag	9.2	1.44	0.99	1.00
D	1.70	1.43	1.45	0.19 lead	6.7	1.52	0.99	0.99
		2.00	2.10	0.20 lead	3.6	1.50	0.99	0.99
E	1.57	1.60	1.67	0.32 lag	22.3	1.57	0.96	0.98

Table 8 Comparison of power quality, near rated power and cooling

Type	P_{nom}, kW	*P*, kW	*S*, kVA	*Q*, kVAR	I_{THD}, %fund.	CF	PF	DPF
*A*25	0.60	0.59	0.76	0.28 lag	60.9	2.03	0.77	0.90
*A*50	1.55	1.60	1.63	0.18 lead	17.2	1.60	0.98	0.99
B	1.72	1.65	1.68	0.12 lead	17.5	1.54	0.98	1.00
C	1.70	1.60	1.62	0.12 lag	12.2	1.44	0.99	1.00
D	1.66	1.65	1.66	0.22 lead	5.2	1.52	0.99	0.99
E[a]	1.37	1.04	1.11	0.21 lag	30.7	1.67	0.94	0.98

[a]Unit *E* could not be made to draw rated power on the cooling cycle (possibly because of an internal fault) although on heating mode rated power could be achieved.

This is an open access article published by the IET under the Creative Commons Attribution-NonCommercial License (http://creativecommons.org/licenses/by-nc/3.0/)